IEEE Access
Multidisciplinary ⁝ Rapid Review ⁝ Open Access Journal

Received 29 July 2024, accepted 22 August 2024, date of publication 26 August 2024, date of current version 5 September 2024.

Digital Object Identifier 10.1109/ACCESS.2024.3450194

RESEARCH ARTICLE

Efficient FPGA Realization of the Memristive Wilson Neuron Model in the Face of Electromagnetic Interference

MOHAMMED ABDEL-HAFEZ[1], (Senior Member, IEEE), FAWWAZ HAZZAZI[2], (Member, IEEE), LEWIS NKENYEREYE[3], IBRAHIM MAHARIQ[4,5], (Member, IEEE), MUHAMMAD AKMAL CHAUDHARY[6], (Senior Member, IEEE), AND MAHER ASSAAD[6]

[1]Department of Electrical and Communication Engineering, United Arab Emirates University, Al Ain, United Arab Emirates
[2]Department of Electrical Engineering, College of Engineering, Prince Sattam Bin Abdulaziz University, Al-Kharj 11492, Saudi Arabia
[3]Department of Computer and Information Security, Sejong University, Seoul 05006, South Korea
[4]Electrical and Computer Engineering Department, Gulf University for Science and Technology, Mishref 32093, Kuwait
[5]Department of Medical Research, China Medical University Hospital, China Medical University, Taichung 404, Taiwan
[6]Department of Electrical and Computer Engineering, College of Engineering and Information Technology, Ajman University, Ajman, United Arab Emirates

Corresponding authors: Mohammed Abdel-Hafez (mhafez@uaeu.ac.ae) and Lewis Nkenyereye (nkenyele@sejong.ac.kra)

ABSTRACT Hardware implementation of new neuron models or improved conventional neuron models has made a significant contribution to neuromorphic development. One of the important factors considered to improve the conventional neuron models is to explore the impact of electromagnetic energy on neurons. In this work the efficient FPGA implementation of memristive Wilson (MW) neuron model using two approximate MW model is presented. For the first approximate MW (AMW1) model in a hybrid method, piecewise linear (PWL) and CORDIC functions have been used to provide a multiplierless and accurate model. The PWL approximation method is used to provide the second approximate MW (AMW2) model. Results of the FPGA implementation for both the MW and AMW models illustrate that, the AMW1 model with an overall saving of 79%, and the AMW2 model with an overall saving of 69% are appropriate options for large scale implementations. The average NRMSE for the AMW1 model is 0.57%, while for the AMW2 model it is 1.23%. The maximum frequency of AMW2 model is 91.5% better than AMW1 model and realizes high frequency implementation.

INDEX TERMS Memristive Wilson neuron model, piecewise linear model, electromagnetic radiation, hyperbolic transformation.

I. INTRODUCTION

The brain, with all its complexity, is made up of billions of neurons. To understand the complex functioning of the brain, one must understand the structure and performance of neurons [1], [2], as well as how neurons communicate through synaptic pathways [3], [4]. Therefore, various mathematical models have been presented for neurons. These models often consist of coupled differential equations that relate the main variables of a neuron [5], [6], [7], [8], [9], [10], [11], [12], [13], [14], [15]. Based on the resemblance of the neuron model to an actual neuron, the ability to produce various output patterns and the level of computational complexity, neuron models can be categorized into three distinct groups. The first category includes basic biological models whose parameters are calculated based on the measurable variables of neurons. Complex and precise models such as Hodgkin-Huxley [5], [6] or simple and descriptive models such as Integrate and Fire [7], [8] are in this category. The second category is related to non-biological models whose parameters are defined in such a way as to generate diverse spiking patterns. The most famous model of this category is Izhikevich neuron model [9], [10]. The third category includes hybrid models, which increase the benefits

The associate editor coordinating the review of this manuscript and approving it for publication was Ludovico Minati.

of the obtained model by combining the equations of two different neuron models [16], [17].

Every since the very first neuron models emerged, the research community has worked on new and improved models to reduce computational complexity and more closely describe neuronal dynamics. In general, neural models are fine-tuned to enhance the performance of one of the following:

- Implementing neuron models in hardware to enable the extensive deployment of such models on a large scale. This hardware implementation is being pursued in analog [18], [19] and digital form, and among the digital options, FPGA [20], [21] with its extensive capabilities is commonly used due to its flexibility.
- Use of neuron models in spiking neural networks [22], [23], [24].
- Software simulation of neuron models on a large scale to obtain a software of brain or on a small scale to study neural cells for correctly understanding their behavior to elucidate some common brain diseases [25], [26] or to connect the brain to external hardware.

This paper investigates a memristive Wilson model [14] to show an improvement over the 2D Wilson [27], [28] model. It should be noted that this improved model considers the effect of electromagnetic coupling [29] as a very important environmental factor and thus improves the neurodynamics of the Wilson model. From the practical point of view, this paper implements the improved MW model on FPGA for the first time and two approximation of the improved MW model is presented to reduce the overhead of the hardware implementation and to get closer to large-scale hardware implementation. The arrangement of this paper is outlined as follows. The MW neuron model is introduced in Section II. AMW1 and AMW2 models are presented in Section III as two approximations of the original MW model. Section IV discusses the behavior of an individual neuron through dynamic analysis. The interaction between two coupled MW/AMW neurons are explored in Section V. The FPGA implementation of the MW and AMW models are showcased in Section VI, and Section VII concludes this paper.

II. MEMRISTIVE WILSON NEURON MODEL

In 1952, a detailed and complex model of the neuron was developed by Hodgkin and Huxley. Subsequent models primarily consist of a simplified version of the Hodgkin-Huxley model. The 2D Wilson model, which is a simplified form of Hodgkin-Huxley's model, is described by

$$\begin{cases} \dfrac{dv}{dt} = \dfrac{1}{C_m}(-m_\infty(v)(v-E_{\mathrm{Na}}) - g_K r(v-E_{\mathrm{K}}) + I_{\mathrm{st}}) \\ \dfrac{dr}{dt} = \dfrac{1}{\tau_r}(-r + r_\infty(v)). \end{cases} \tag{1}$$

In system (1), $m_\infty(v)$ and $r_\infty(v)$ define the Na^+ ion activation system and equilibrium state of recovery variable which are formulated as

$$\begin{cases} m_\infty(v) = 17.8 + 47.6v + 33.8v^2 \\ r_\infty(v) = 1.24 + 3.7v + 3.2v^2, \end{cases} \tag{2}$$

where v represents the neuron's membrane potential and r is the recovery variable. C_m, E_{Na}, E_{K}, g_{K}, I_{st} and τ_r denote the membrane capacitor, reversal potentials of Na^+ ion channel, reversal potentials of K^+ ion channel, the maximal conductance of K^+ ion channel, external stimulus current and activation time of K^+ ion channel, respectively. To enhance the capability of the Wilson neuron model in simulating real-world phenomena, the effect of electromagnetic (EM) radiation is incorporated into the Wilson model by employing a flux-controlled memristor. The conversion of the 2D Wilson neuron model into a memristive model involves the incorporation of the effect of EM radiation through the addition of the EM induction current $I_{mf} = kW(\phi)v = k(a - b|\phi|)v$ to the system (1). In this equation, ϕ is the EM flux variable, $W(\phi) = a - b|\phi|$ represents the memductance of the memristor. The equations of memristive Wilson neuron model are as

$$\begin{cases} \dfrac{dv}{dt} = \dfrac{1}{C_m}(-m_\infty(v)(v-E_{\mathrm{Na}}) - g_K r(v-E_{\mathrm{K}}) \\ \qquad + I_{\mathrm{st}} + k(a-b|\phi|)) \\ \dfrac{dr}{dt} = \dfrac{1}{\tau_r}(-r + r_\infty(v)) \\ \dfrac{d\phi}{dt} = \dfrac{1}{\tau_\phi}(k_1 v - \phi), \end{cases} \tag{3}$$

in which, τ_ϕ defines the time scale of the EM flux changes.

Formulating the v-nullcline and r-nullcline is accomplished using the equilibrium value of $\phi = k_1 v$.

$$\begin{cases} r_{n1} = \dfrac{1}{26(v+1)}(-33.8v^3 - 30.7v^2 + 6v + 14.9 - 18|v|) \\ r_{n2} = 3.2v^2 + 3.7v + 1.24 \end{cases} \tag{4}$$

Based on the system (4), nullclines of the v and r are illustrated in Fig. 1.

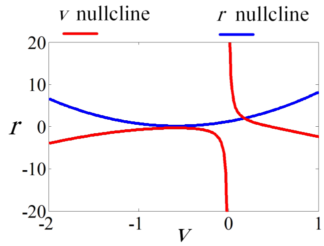

FIGURE 1. The nullclines for the MW system based on the $C_m = 1$, $E_{\mathrm{Na}} = 0.5$, $g_K = 26$, $E_{\mathrm{K}} = -1$, $I_{\mathrm{st}=0}$, $\tau_r = 4$, and $\tau_\phi = 0.5$, $a = 1$, $b = 3$, $k = 6$ and $k_1 = 1$.

III. PROPOSED MULTIPLIERLESS MW MODELS

The nonlinear structure and the presence of multiple multiplications in the equations of system (3) increase the FPGA implementation cost of MW model and also decrease its processing frequency. In order to reduce FPGA

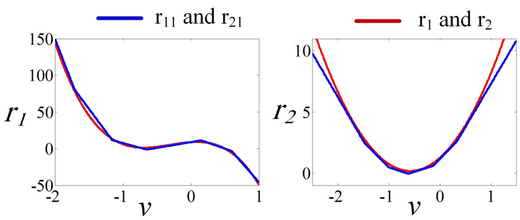

FIGURE 2. PWL approximation of r_1 and r_2 for AMW1 model.

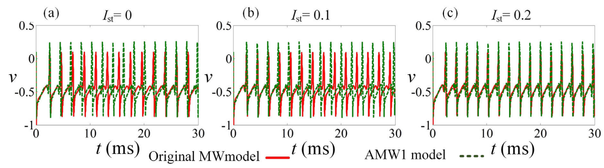

FIGURE 3. Output simulation results for the MW and AMW1 models. (a) $I_{st} = 0$, (b) $I_{st} = 0.1$, (c) $I_{st} = 0.2$.

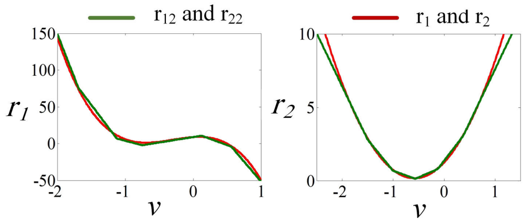

FIGURE 4. PWL approximation of r_1 and r_2 for AMW2 model.

implementation costs and increase the operating frequency, it has been tried to provide two approximate models for the original MW model, each of which meets different levels of accuracy and speed and can be used for different hardware implementation scenarios.

A. FIRST APPROXIMATE MW MODEL

As seen in Fig. 2, AMW1 model approximates $r_1 = -33.8v^3 - 30.7v^2 + 6v + 8.9$ and $r_2 = 3.2v^2 + 3.7v + 1.24$ with 6 lines using the piecewise linear (PWL) approximation method. Equations containing multiplication in the original MW system are approximated by *cosh* expressions. The r_1 and r_2 are approximated in AMW1 model by r_{11} and r_{21}.

$$r_{11} = \begin{cases} -107.75v + 58.609375 & \text{if } v > 0.59375 \\ -32.75v + 14.078125 & \text{if } 0.125 < v < 0.59375 \\ 15.25v + 8.078125 & \text{if } -0.625 < v < 0.125 \\ -26.25v - 17.859375 & \text{if } -1.125 < v < -0.625 \\ -124.25v - 128.109375 & \text{if } -1.75 < v < -1.125 \\ -238.25v - 327.609375 & \text{if } v < -1.75 \end{cases} \tag{5}$$

$$r_{21} = \begin{cases} 7.0625v + 0.15625 & \text{if } v > 0.375 \\ 4.3125v + 1.1875 & \text{if } -0.125 < v < 0.375 \\ 1.3125v + 0.8125 & \text{if } -0.625 < v < -0.125 \\ -1.4375v - 0.90625 & \text{if } -1 < v < -0.625 \\ -4.1875v - 3.65625 & \text{if } -1.5 < v < -1 \\ -7.1875v - 8.15625 & \text{if } v < -1.5 \end{cases} \tag{6}$$

and by converting r_{11} and r_{21} into the form of absolute value functions, AMW1 model is formulated as

$$\begin{cases} \dfrac{dv}{dt} = (-134.5 - 173v - 37.5|v - 0.59375| \\ \qquad - 24|v - 0.125| + 20.75|v + 0.625| + 49|v \\ \qquad + 1.125| + 57|v + 1.75| + I_{st} \\ \qquad + (0.5g_K cosh(r - v - 1)) - 0.5g_K cosh(r + v + 1)) \\ \qquad + akv + 0.5bk(cosh(v - |\phi|) - cosh(v + |\phi|)) \\ \dfrac{dr}{dt} = 0.25(-0.0625v + 1.375|v + 1| \\ \qquad + 1.375|v - 0.375| + 1.5|v + 0.125| \\ \qquad + 1.375|v + 0.625| + 1.5|v + 1.5| - r - 4) \\ \dfrac{d\phi}{dt} = 4(k_1 v - \phi) \end{cases} \tag{7}$$

Fig. 3 shows the spiking simulation results of the AMW1 and MW models, based on the distinct stimuli. In order to check the behavioral similarity of the AMW1 model with the MW model, we must check the response of both models to the different stimulus current to see if they have the same behavior in terms of the spiking type and the location of the spikes. As shown in Fig. 3, both AMW1 and MW models have responded tonic spiking to $I_{st} = 0$, $I_{st} = 0.1$ and $I_{st} = 0.2$, and the similarity of spike timing in all three simulations is acceptable. In $I_{st} = 0.2$, this similarity has reached its peak.

B. SECOND APPROXIMATE MW MODEL

As can be seen in Fig. 4, in AMW2 model, r_1 and r_2 are again approximated with 6 lines by r_{12} and r_{22} (r_{12} and r_{22} are a slight different compared to r_{11} and r_{21}). According to the noticeable matching of v and ϕ graphs which is evident in Fig. 5, the $v|\phi|$ term can be approximated by $v|v|$ and finally by the linear relationship of $0.715v$. The equations of AMW2 model are described by (8).

$$\begin{cases} \dfrac{dv}{dt} = -172.75v - 37|v - 0.5625| - 24.5|v - 0.125| \\ \qquad + 19.5|v + 0.75| + 49|v + 1.125| + 57.5|v \\ \qquad + 1.6875| - 0.5r - 11(v + 1) + I_{st} + kav \\ \qquad - kb(0.75\phi) - 134 \\ \dfrac{dr}{dt} = (-r - 3.875 + 1.5|v + 1| + 1.375|v - 0.375| \\ \qquad + 1.5|v + 0.125| + 1.375|v + 0.5625| \\ \qquad + 1.5|v + 1.5|)0.25 \\ \dfrac{d\phi}{dt} = 2(k_1 v - \phi) \end{cases} \tag{8}$$

Fig. 6 explains the output of the AMW2 model and the MW model, showcasing the influence of varying stimulus currents. According to the Fig. 6, both the AMW2 and MW models exhibited tonic spiking in response to $I_{st} = 0$,

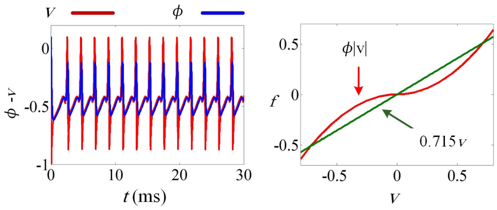

FIGURE 5. Noticeable matching of v and ϕ output patterns and a low cost approximation for $v|\phi|$.

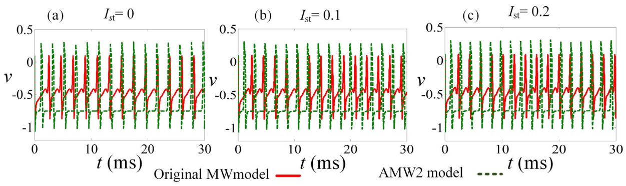

FIGURE 6. Output simulation results for the MW and AMW2 models (a) $I_{st} = 0$ (b) $I_{st} = 0.1$ (c) $I_{st} = 0.2$.

TABLE 1. Controlling parameters for error analysis.

Parameter Name	C_m	E_{Na}	g_K	τ_r	τ_ϕ	a	b	k	k_1
Parameter Value	1	0.5	29.3	4	0.5	1	3.1	6.02	1

$I_{st} = 0.1$ and $I_{st} = 0.2$. The similarity of the spike timing in all three simulations was found to be satisfactory.

C. ERROR ANALYSIS

To validate the proposed models, one of the methods involves computing the discrepancy between the output patterns of the proposed AMW models and the MW model. The output patterns of the original MW model compare with the AMW models using root mean square error (RMSE) and the normalized RMSE (NRMSE). If v_{MW} and v_{AMW} represent the membrane potential of the MW model and AMW models, RMSE and NRMSE are formulated as

$$\mathrm{RMSE}(v_{\mathrm{AMW}}, v_{\mathrm{MW}}) = \sqrt{\frac{\sum_{i=1}^{n}(v_{\mathrm{AMW}} - v_{\mathrm{MW}})^2}{n}} \tag{9}$$

$$\mathrm{NRMSE} = \frac{\mathrm{RMSE}}{v_{\max} - v_{\min}}. \tag{10}$$

The controlling parameters for error calculation of AMW models are illustrated in Table 1.

The erreor analysis results for AMW models are depicted in Table 2. The AMW1 model demonstrates a mean NRMSE of 0.57%, while the AMW2 model exhibits a mean NRMSE of 1.23%.

IV. SINGLE NEURON DYNAMIC ANALYSIS

In order to investegate the dynamic characteristics of the MW and AMW models, the value of ϕ is assumed to be constant, and in the remained 2D system, interactions of the v-nullclines and r-nullclines explain the transition between the resting and spiking modes [17]. The computation of the Jacobian matrix for the MW model is performed using the

TABLE 2. Error analysis results.

I_{st}	AMW1		AMW2	
	RMSE	NRMSE%	RMSE	NRMSE%
0.3	0.24	0.2	0.45	1.97
0.35	0.24	0.6	0.45	0.7
0.4	0.24	0.87	0.46	0.34
0.45	0.24	0.23	0.45	0.54
0.5	0.24	0.08	0.46	1.25
0.55	0.24	1.48	0.47	2.62
Mean Error	0.24	0.57	0.45	1.23

TABLE 3. Equilibrium points of the original MW and proposed AMW models.

I_{st}	MW Model		AMW1 model		AMW2 model	
	EP Type	EP Value	EP Type	EP Value	EP Type	EP Value
0	NS	(-0.958, 0.633)	NS	(-0.876, 0.299)	NS	(-1.04, 0.859)
0.2	NS	(-0.95, 0.620)	NS	(-0.868, 0.288)	NS	(-1.03, 0.828)
0.4	NS	(-0.947, 0.607)	NS	(-0.86, 0.277)	NS	(-1.02, 0.796)

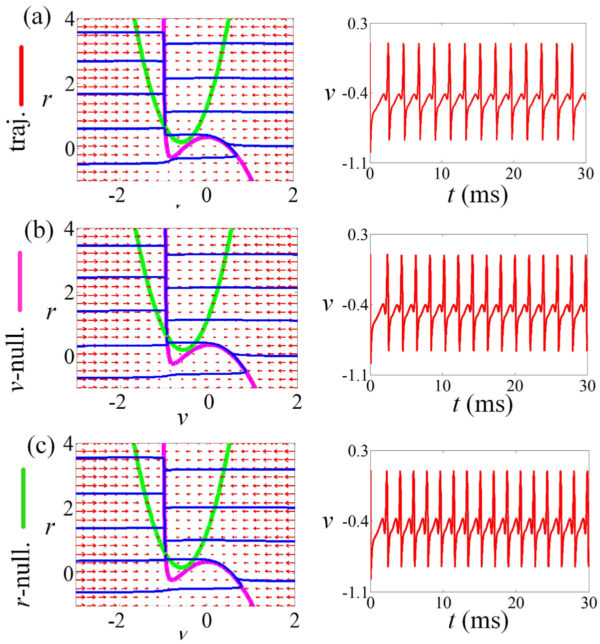

FIGURE 7. Dynamic analysis of the original MW model for (a) $I_{st} = 0$. (b) $I_{st} = 0.2$. (c) $I_{st} = 0.4$.

following equation.

$$J_{MW} = \begin{bmatrix} \frac{\partial \dot{v}}{\partial v} & \frac{\partial \dot{v}}{\partial r} \\ \frac{\partial \dot{r}}{\partial v} & \frac{\partial \dot{r}}{\partial r} \end{bmatrix} \tag{11}$$

where

$$\begin{cases} \frac{\partial \dot{v}}{\partial v} = \frac{1}{C_m}(-101.4v^2 - 61.4v + 6) \\ \frac{\partial \dot{v}}{\partial r} = \frac{1}{C_m}(-26v - 26) \\ \frac{\partial \dot{r}}{\partial v} = \frac{1}{\tau_r}(6.4v + 3.7) \\ \frac{\partial \dot{r}}{\partial r} = \frac{-1}{\tau_r} \end{cases} \tag{12}$$

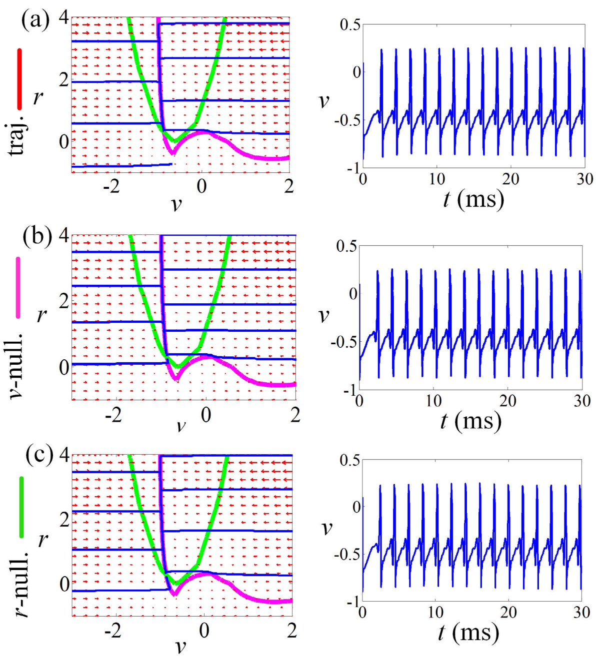

FIGURE 8. Dynamic analysis of the AMW1 model for (a) $I_{st} = 0$. (b) $I_{st} = 0.2$. (c) $I_{st} = 0.4$.

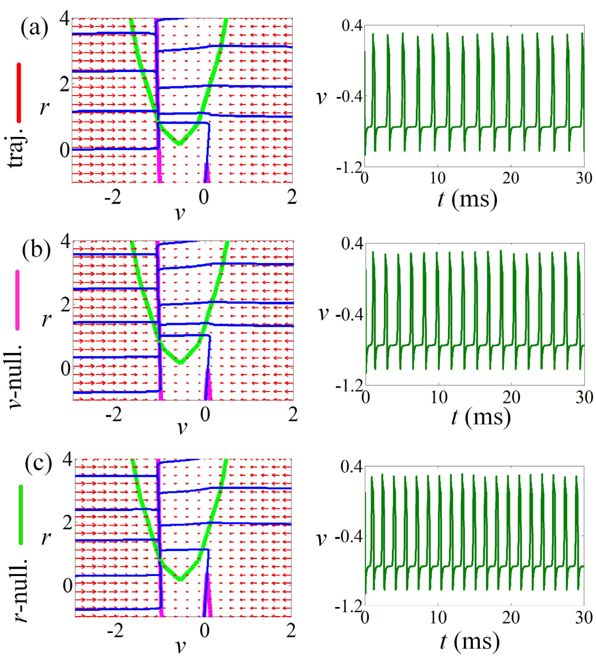

FIGURE 9. Dynamic analysis of the AMW2 model for (a) $I_{st} = 0$. (b) $I_{st} = 0.2$. (c) $I_{st} = 0.4$.

The fixed points which are satisfied the $\frac{\partial \dot{v}}{\partial v} + \frac{\partial \dot{r}}{\partial r} < 0$ are stable, otherwise, they are unstable. The phase portraits of MW, AMW1 and AMW2 models for various I_{st} are illustrated in Fig. 7, Fig. 8 and Fig. 9. Based on the dynamic alalysis results, equilibrium points (EPs) type and EPs value of MW and AMW models are presented in Table 3. The likeness between the MW and AMW models regarding the EP type (under the same stimulation conditions, EP type of the MW and AMW models is nodal sink (NS)) and EP value, confirms the similarity of the excitability of the MW and the proposed AMW models.

V. SYNAPTIC COUPLING OF TWO MW/AMW NEURONS

The performance of the complex network of the brain is dependent on the synaptic connection between neurons. Synapse is a bioelectrical or biochemical signaling pathway between neurons that can be formulated as [20].

$$\begin{cases} \tau_s \dfrac{dz}{dt} = [1 + \tanh(S_s(v_{pr} - h_s))](1 - z) - \dfrac{z}{d_s} \\ I_{syn} = k_s(z - z_0), \end{cases} \tag{13}$$

In the synaptic coupling of two neurons, when the presynaptic neuron reaches the threshold voltage, according to the parameters of the synapse function, a current pulse is sent to the postsynaptic neuron and establishes the connection between the two neurons. If the synaptic coupling between two MW neurons is similar in behavior of the synaptic coupling of two AMW neurons, it is another confirmation of the compatibility of the proposed AMW models with the MW model. The coupling between two original MW neurons is formulated as

$$\begin{cases} \dfrac{dv_{pr}}{dt} = \dfrac{1}{C_m}(-m_\infty(v_{pr})(v_{pr} - E_{Na}) \\ \qquad - g_K r(v_{pr} - E_K) + I_{st} + k(a - b|\phi_{pr}|)) \\ \dfrac{dr_{pr}}{dt} = \dfrac{1}{\tau_r}(-r_{pr} + r_\infty(v_{pr})) \\ \dfrac{d\phi_{pr}}{dt} = \dfrac{1}{\tau_\phi}(k_1 v_{pr} - \phi_{pr}), \\ \tau_s \dfrac{dz}{dt} = [1 + \tanh(S_s(v_{pr} - h_s))](1 - z) - \dfrac{z}{d_s} \\ I_{syn} = k_s(z - z_0) \\ \dfrac{dv_{po}}{dt} = \dfrac{1}{C_m}(-m_\infty(v_{po})(v_{po} - E_{Na}) \\ \qquad - g_K r(v_{po} - E_K) + I_{syn} + k(a - b|\phi_{po}|)) \\ \dfrac{dr_{po}}{dt} = \dfrac{1}{\tau_r}(-r_{po} + r_\infty(v_{po})) \\ \dfrac{d\phi_{po}}{dt} = \dfrac{1}{\tau_\phi}(k_1 v_{po} - \phi_{po}), \end{cases} \tag{14}$$

where v_{pr}, r_{pr} and ϕ_{pr} represent the presynaptic neuron variables and v_{po}, r_{po} and ϕ_{po} define the postsynaptic neuron variables.

Simulation results of two coupled MW/AMW neurons when exposed to different input current from the presynaptic neuron are illustrated in Fig. 10. As the stimulus current increases, the synchronization decreases and the full synchronization state occurs for the $I_{st} = 0.01$ and $k_s = 0.5$.

Investigation of the neuron network behavior is very essential. As it depicted in Fig. 11, a network scale of MW and AMW neurons using 1000 randomly connected neurons, are simulated and the raster plot results show a good agreement between MW and AMW networks behavior.

Fig. 12 simulates the random firing activity of the MW and AMW neurons. The relative error (RE) of the m^{th} spike for the

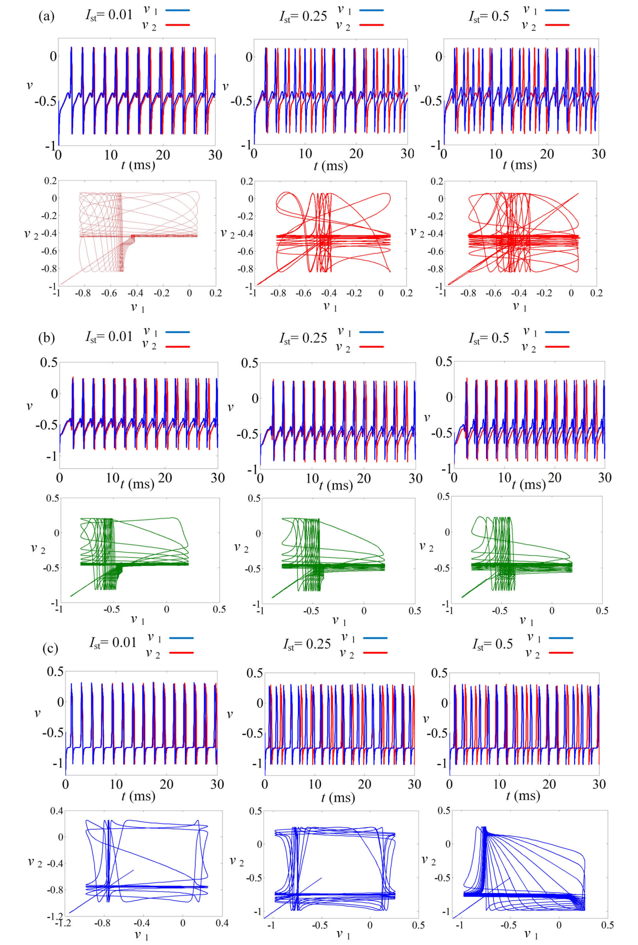

FIGURE 10. Phase portraits and spiking patterns of two interconnected original MW, AMW1, and AMW2 neurons when exposed to different input excitation current from the presynaptic neuron. (a) Two coupled MW neurons. (b) Two coupled AMW1 neurons. (c) Two coupled AMW2 neurons. (v_1/v_2 represents the membrane potential of the presynaptic/postsynaptic neuron).

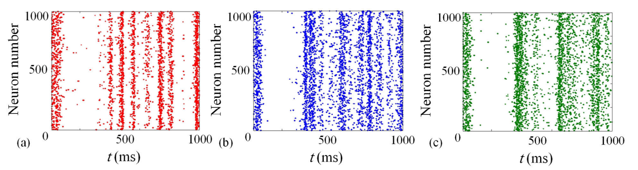

FIGURE 11. Network activity of 1000 randomly connected neurons of the (a) Original MW model. (b) AMW1 model. (c) AMW2 model.

n^{th} AMW neurons is defined by $\left|\frac{\Delta t_{nm}}{t_{nm}}\right|$ [20], and then average value of these calculations is obtained as mean relative error (MRE). The MRE of a set of randomly connected 1000 neurons for the proposed AMW1 and AMW2 models are 6.7% and 8.3% respectively.

$$\mathrm{MRE}(\%) = \frac{\sum_{n=1}^{i}\sum_{m=1}^{j}\left|\frac{\Delta t_{nm}}{t_{nm}}\right|}{i \times j} \times 100 \qquad (15)$$

VI. FPGA IMPLEMENTATION

The FPGA implementation paves the way for the large scale implementation of neuron models and finally designing a prototype of a hardware brain. Fig. 13 shows the proposed architecture for FPGA implementation of the AMW models. Input unit, control unit, neuron unit and output unit are the main subsystems in the proposed architecture. The input unit provides the required space to store the input parameters of the system. The control unit approximates the original MW model with AMW2 model using PWL approximation method. The CORDIC part of FPGA along with PWL method are applied by control unit to approximate AMW1 model. Within this subsystem, comparators utilize the values of v and other constants to choose the approximate function of v using multiplexers. The approximations obtained from the control unit are used in the neuron unit and it calculates the digital values of the variables using the designed pipelines. The output unit, while storing the calculated values for the digital variables, provides the conditions for calling these variables to display the output pattern.

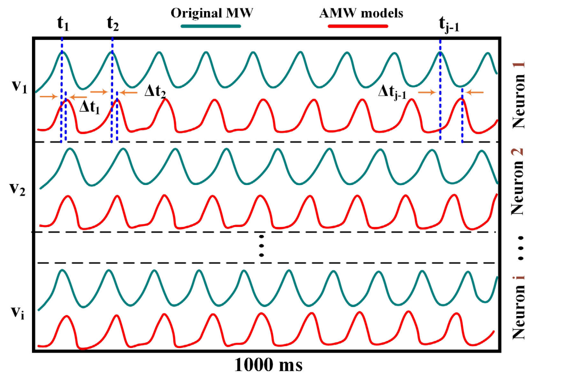

FIGURE 12. Simulated firing plot of the original MW and proposed AMW models.

A. SYSTEM DISCRETIZATION AND PIPELINE DESIGN

The digital implementation of differential equations requires the discretization of these equations, and it has been realized using Euler method [1]. The discrete type of AMW1 and AMW2 equations are formulated as (16) and (17).

$$d_1 = \begin{cases} v[n+1] = v[n] + d_t(-134.5 - 173v[n] \\ \quad - 37.5|v[n] - 0.59375| - 24|v[n] - 0.125| \\ \quad + 20.75|v[n] + 0.625| + 49|v[n] + 1.125| \\ \quad + I_{\mathrm{st}} + (0.5g_K cosh(r[n] - v[n] - 1)) \\ \quad - 0.5g_K cosh(r[n] + v[n] + 1)) \\ \quad + akv[n] + 0.5bk(cosh(v[n] - |\phi|) \\ \quad - cosh(v[n] + |\phi|) + 57|v[n] + 1.75|) \\ r[n+1] = r[n] + 0.25d_t(-0.0625v[n] \\ \quad + 1.375|v[n] + 1| + 1.375|v[n] - 0.375| \\ \quad + 1.5|v[n] + 0.125| + 1.375|v[n] + 0.625| \\ \quad + 1.5|v[n] + 1.5| - r[n] - 4) \\ \phi[n+1] = 4d_t(k_1 v[n] - \phi[n]) + \phi[n] \end{cases} \qquad (16)$$

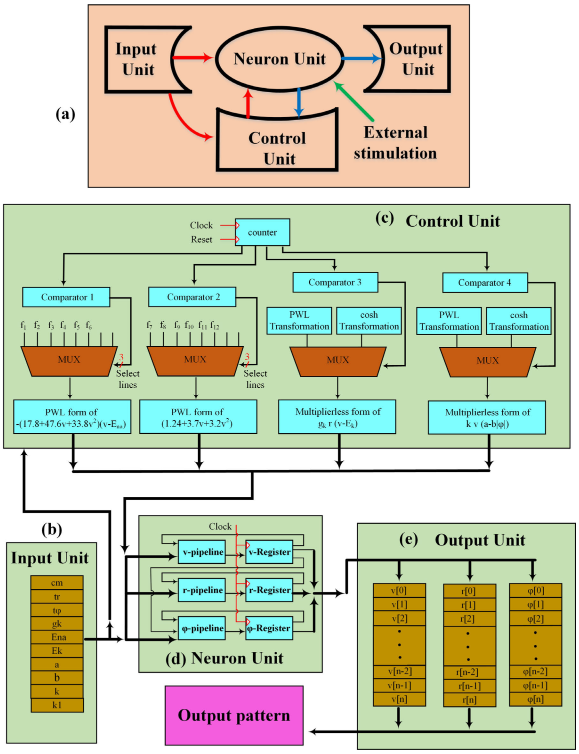

FIGURE 13. Proposed architecture of the digital AMW1 and AMW2 models. (a) general overview (b) The Input Unit. (c) Control Unit. (d) Neuron units (e) Output unit.

$$d_2 = \begin{cases} v[n+1] = v[n] + d_t(I_{\mathrm{st}} - 172.75v[n] \\ \qquad - 37|v[n]-0.5625| - 24.5|v[n]-0.125| \\ \qquad + 19.5|v[n]+0.75| + 49|v[n]+1.125| \\ \qquad + 57.5|v[n]+1.6875| - 0.5r[n] + kav[n] \\ \qquad - 11(v[n]+1) - kb(0.75\phi[n]) - 134) \\ r[n+1] = 0.25d_t(-r[n] - 3.875 \\ \qquad + 1.5|v[n]+1| + 1.375|v[n]-0.375| \\ \qquad + 1.5|v[n]+0.125| + 1.375|v[n] \\ \qquad + 0.5625| + 1.5|v[n]+1.5|) + r[n] \\ \phi[n+1] = 2d_t(k_1 v[n] - \phi[n]) + \phi[n] \end{cases} \tag{17}$$

The coefficients of AMW1 and AMW2 equations are chosen in such a way that they can be replaced by the sum of powers of 2 and finally they can be implemented with shift and add units. Pipeline of AMW1 model is designed based on the (16) and is depicted on Fig. 14. As it illustrated in Fig. 15, digital pipeline of the AMW2 model has presented based on the (17).

B. BIT WIDTH DETERMINATION

simulation results of the AMW1 and AMW2 models shows the following variation for v, r, ϕ and I_{st}.

$$\begin{cases} 0 < I_{\mathrm{st}} < 0.5 \\ -1 < v < 0.5 \\ 0.2 < r < 0.8 \\ -0.8 < \phi < 0.1 \end{cases} \tag{18}$$

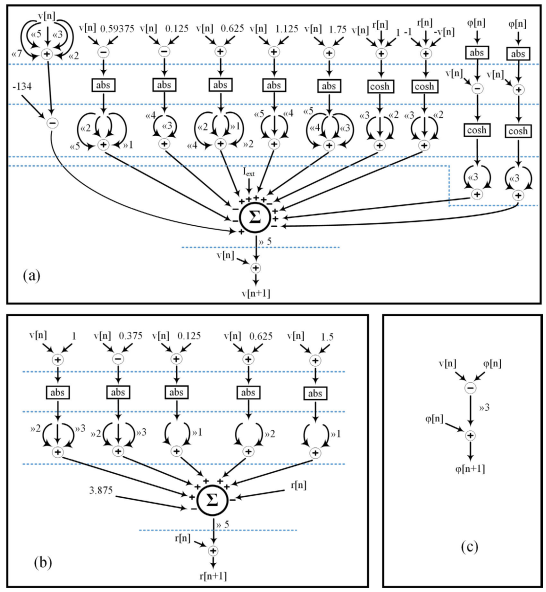

FIGURE 14. AMW1 pipeline for (a) v variable (b) r variable (c) ϕ variable.

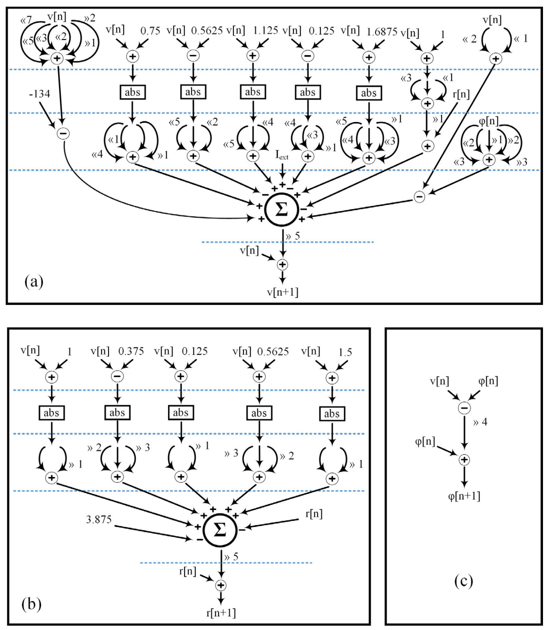

FIGURE 15. AMW2 pipeline for (a) v variable (b) r variable (c) ϕ variable.

Based on the range of variables, parameters value, maximum shifts in the pipeline diagram, the bit width (BW) is calculated as follows.

- The Maximum of (A, B) is considered as BW of integer part. A is the maximum left shifts (7 bits) in the pipline structure and B represents the highest value among the variables and parameters of the AMW models (5 bits for $g_k = 26$).
- The Maximum of (C, D) is considered as BW of fraction part. C is the maximum right shifts (8 bits) in the pipline structure and D corresponds to the minimum value within the variables and parameters of the AMW models (5 bits for $\phi = 0.1$).

TABLE 4. Device utilization for the original MW, AMW1 and AMW2 models.

Resources	Original Model	AMW1 Model	AMW2 Model
Slice LUTs (12480)	361(2.8%)	6.19 (4.9%)	1333 (10.7%)
Slice Register (12480)	341 (2.7%)	322 (2.6%)	852 (6.8%)
Bonded IOBs (172)	29 (16.8%)	18 (10.5%)	18 (10.5%)
DSP48Es (24)	14 (58.3%)	0 (0 %)	0 (0 %)
BUFG/BUFGCTRLs (32)	1 (3%)	1 (3%)	1 (3%)
Max frequency	139.06 MHz	116.63 MHz	223.4 MHz
Overall saving	16.4%	79 %	69%

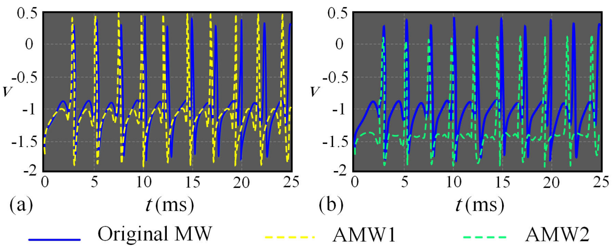

FIGURE 16. Digital output of implemented AMW1, AMW2 and original MW models (a) spiking pattern of AMW1 and original MW (b) spiking pattern of AMW2 and original MW.

- One bit is defined as sign bit and inorder to prevent the possible overflow, one additional bit is considered.

Therefore, the BW of the AMW models is 17.

C. IMPLEMENTATION RESULTS

Fig. 16 illustrates the digital created patterns of the AMW models and the MW model implemented on a Virtex-5 XC5VLX20T FPGA. Digital data are converted by a DAC with 8-bit bitrate and displayed on the oscilloscope. Table 4 presents a comparison of FPGA resource utilization between the MW and AMW models. To compare the results of Table 4, it is important to pay attention to the following points.

- FPGA's resources usage rate. For this purpose, the overal saving criterion has been used [17].
- The limiting factor between hardware resources used by FPGA. The limiting factor is related to the highest utilization percentage among FPGA resources.
- Maximum available frequency in FPGA implementation of a neuron model.

Overall saving is a criterion to show the total percentage of FPGA resources used in the implementation of a neuron model. If we add up the FPGA resources utilizationand and subtract the result from 100, the overall saving of FPGA hardware resources is obtained. A larger overall saving means fewer hardware resources are used. The overall saving of original MW model, AMW1 model and AMW2 model are 16.4%, 79% and 69% respectively and it shows that the original MW model has the highest hardware implementation cost and AMW1 model has the lowest hardware cost. The limiting factor for the MW model is DSP48Es sets with 58.3% utilization, for the AMW1 model is Bonded IOBs with 10.5% and for the AMW1 model is Slice LUTs with 10.7%. This means that the limiting factor allows the FPGA implementation of only one neuron using original MW model and 9 neurons with AMW1 and AMW2 models. Maximum frequency of original MW model is 139.06 MHz, and AMW1 and AMW2 models reache the 116.63 MHz and 223.4 MHz maximum frequency. Therefore, AMW1 model is used when high accuracy and lower hardware implementation cost are needed, but processing speed is a lower priority. AMW2 model with acceptable accuracy and implementation cost, is sutable for high frequency cases and both AMW1 and AMW2 models, with the ability to implement neurons 9 times more than the original MW model, are suitable options for large sclae implementation.

VII. CONCLUSION

In this work a MW neuron model and two approximate MW (AMW1 and AMW2) models are implmented on FPGA platform. AMW1 model using the PWL functions and hyperbolic transformation approximates the orginal MW model. The hardware overhead of the accurate AMW1 model is significantly reduced with an overall saving of 79% but the maximum frequency of this model is 116.63 MHz which shows a lower frequency than the implemented AMW2 and the original MW models. AMW2 model with an overall saving of 69% and the maximum frequency of 223.4 MHz provide a low cost and high frequncy FPGA implementation. The number of neurons that can be implemented by AMW1 and AMW2 models, is 9 times that of the original MW model, which shows these two models are suitable for large scale implementation.

REFERENCES

[1] M. Hayati, M. Nouri, S. Haghiri, and D. Abbott, "A digital realization of astrocyte and neural glial interactions," *IEEE Trans. Biomed. Circuits Syst.*, vol. 10, no. 2, pp. 518–529, Apr. 2016, doi: 10.1109/TBCAS.2015.2450837.

[2] S. Haghiri, A. Ahmadi, and M. Saif, "Complete neuron-astrocyte interaction model: Digital multiplierless design and networking mechanism," *IEEE Trans. Biomed. Circuits Syst.*, vol. 11, no. 1, pp. 117–127, Feb. 2017, doi: 10.1109/TBCAS.2016.2583920.

[3] P. Zhou, X. Zhang, and J. Ma, "How to wake up the electric synapse coupling between neurons?" *Nonlinear Dyn.*, vol. 108, no. 2, pp. 1681–1695, Apr. 2022, doi: 10.1007/S11071-022-07282-0.

[4] M. A. Imani, A. Ahmadi, M. RadMalekshahi, and S. Haghiri, "Digital multiplierless realization of coupled Wilson neuron model," *IEEE Trans. Biomed. Circuits Syst.*, vol. 12, no. 6, pp. 1431–1439, Dec. 2018, doi: 10.1109/TBCAS.2018.2869319.

[5] A. L. Hodgkin and A. F. Huxley, "A quantitative description of membrane current and its application to conduction and excitation in nerve," *J. Physiol.*, vol. 117, no. 4, pp. 500–544, Aug. 1952, doi: 10.1113/JPHYSIOL.1952.SP004764.

[6] Y. Liu, H. H. Iu, and Y. Qian, "Implementation of Hodgkin-Huxley neuron model with the novel memristive oscillator," *IEEE Trans. Circuits Syst. II, Exp. Briefs*, vol. 68, no. 8, pp. 2982–2986, Aug. 2021, doi: 10.1109/TCSII.2021.3066471.

[7] J. Q. Yang, R. Wang, Z. P. Wang, Q. Y. Ma, J. Y. Mao, Y. Ren, X. Yang, Y. Zhou, and S. T. Han, "Leaky integrate-and-fire neurons based on perovskite memristor for spiking neural networks," *Nano Energy*, vol. 74, Aug. 2020, Art. no. 104828, doi: 10.1016/J.NANOEN.2020.104828.

[8] J. Woo, S. H. Kim, K. Han, and M. Choi, "Characterization of dynamics and information processing of integrate-and-fire neuron models," *J. Phys. A, Math. Theor.*, vol. 54, no. 44, Nov. 2021, Art. no. 445601, doi: 10.1088/1751-8121/AC2A54.

[9] E. M. Izhikevich, "Simple model of spiking neurons," *IEEE Trans. Neural Netw.*, vol. 14, no. 6, pp. 1569–1572, Nov. 2003, doi: 10.1109/TNN.2003.820440.

[10] M. S. Feali and A. Hamidi, "Dynamical response of autaptic Izhikevich neuron disturbed by Gaussian white noise," *J. Comput. Neurosci.*, vol. 51, no. 1, pp. 59–69, Feb. 2023, doi: 10.1007/S10827-022-00832-W.

[11] Z. Li, Z. Guo, M. Wang, and M. Ma, "Firing activities induced by memristive autapse in Fitzhugh–Nagumo neuron with time delay," *Int. J. Electron. Commun.*, vol. 142, Dec. 2021, Art. no. 153995, doi: 10.1016/J.AEUE.2021.153995.

[12] S. Zhang, J. Zheng, X. Wang, and Z. Zeng, "A novel no-equilibrium HR neuron model with hidden homogeneous extreme multistability," *Chaos, Solitons Fractals*, vol. 145, Apr. 2021, Art. no. 110761, doi: 10.1016/J.CHAOS.2021.110761.

[13] K. Li, H. Bao, H. Li, J. Ma, Z. Hua, and B. Bao, "Memristive rulkov neuron model with magnetic induction effects," *IEEE Trans. Ind. Informat.*, vol. 18, no. 3, pp. 1726–1736, Mar. 2022, doi: 10.1109/TII.2021.3086819.

[14] Q. Xu, Z. Ju, S. Ding, C. Feng, M. Chen, and B. Bao, "Electromagnetic induction effects on electrical activity within a memristive Wilson neuron model," *Cognit. Neurodynamics*, vol. 16, no. 5, pp. 1221–1231, Oct. 2022, doi: 10.1007/S11571-021-09764-0.

[15] M. Nouri, M. Hayati, T. Serrano-Gotarredona, and D. Abbott, "A digital neuromorphic realization of the 2-D Wilson neuron model," *IEEE Trans. Circuits Syst. II, Exp. Briefs*, vol. 66, no. 1, pp. 136–140, Jan. 2019, doi: 10.1109/TCSII.2018.2852598.

[16] H. A. Brooks and P. C. Bressloff, "Quasicycles in the stochastic hybrid morris-lecar neural model," *Phys. Rev. E, Stat. Phys. Plasmas Fluids Relat. Interdiscip. Top.*, vol. 92, no. 1, Jul. 2015, Art. no. 012704, doi: 10.1103/PHYSREVE.92.012704.

[17] S. Majidifar, M. Hayati, M. R. Malekshahi, and D. Abbott, "Low cost digital implementation of hybrid FitzHugh Nagumo–Morris lecar neuron model considering electromagnetic flux coupling," *IEEE Trans. Biomed. Circuits Syst.*, vol. 16, no. 6, pp. 1366–1374, Dec. 2022, doi: 10.1109/TBCAS.2022.3214851.

[18] G. Indiveri, E. Chicca, and R. Douglas, "A VLSI array of low-power spiking neurons and bistable synapses with spike-timing dependent plasticity," *IEEE Trans. Neural Netw.*, vol. 17, no. 1, pp. 211–221, Jan. 2006, doi: 10.1109/TNN.2005.860850.

[19] A. Basu, S. Ramakrishnan, C. Petre, S. Koziol, S. Brink, and P. E. Hasler, "Neural dynamics in reconfigurable silicon," *IEEE Trans. Biomed. Circuits Syst.*, vol. 4, no. 5, pp. 311–319, Oct. 2010, doi: 10.1109/TBCAS.2010.2055157.

[20] S. Majidifar, M. Hayati, M. R. Malekshahi, and D. Abbott, "FPGA implementation of memristive Hindmarsh–Rose neuron model: Low cost and high-performing through hybrid approximation," *Int. J. Electron. Commun.*, vol. 172, Dec. 2023, Art. no. 154968, doi: 10.1016/J.AEUE.2023.154968.

[21] A. Ghiasi and A. Zahedi, "Field-programmable gate arrays-based morris-lecar implementation using multiplierless digital approach and new divider-exponential modules," *Comput. Electr. Eng.*, vol. 99, Apr. 2022, Art. no. 107771, doi: 10.1016/J.COMPELECENG.2022.107771.

[22] M. Yao, G. Zhao, H. Zhang, Y. Hu, L. Deng, Y. Tian, B. Xu, and G. Li, "Attention spiking neural networks," *IEEE Trans. Pattern Anal. Mach. Intell.*, vol. 1, no. 2, pp. 1–18, Jul. 2023, doi: 10.1109/TPAMI.2023.3241201.

[23] R. Rajagopal, R. Karthick, P. Meenalochini, and T. Kalaichelvi, "Deep convolutional spiking neural network optimized with arithmetic optimization algorithm for lung disease detection using chest X-ray images," *Biomed. Signal Process. Control*, vol. 79, Jan. 2023, Art. no. 104197, doi: 10.1016/J.BSPC.2022.104197.

[24] M. Mirsadeghi, M. Shalchian, S. R. Kheradpisheh, and T. Masquelier, "Spike time displacement-based error backpropagation in convolutional spiking neural networks," *Neural Comput. Appl.*, vol. 35, no. 21, pp. 15891–15906, Apr. 2023, doi: 10.1007/S00521-023-08567-0.

[25] J. H. Kim, J.-K. Lee, H.-G. Kim, K.-B. Kim, and H. R. Kim, "Possible effects of radiofrequency electromagnetic field exposure on central nerve system," *Biomolecules Therapeutics*, vol. 27, no. 3, pp. 265–275, May 2019, doi: 10.4062/BIOMOLTHER.2018.152.

[26] L. Hardell and C. Sage, "Biological effects from electromagnetic field exposure and public exposure standards," *Biomed. Pharmacotherapy*, vol. 62, no. 2, pp. 104–109, Feb. 2008, doi: 10.1016/J.BIOPHA.2007.12.004.

[27] Q. Xu, Z. Ju, C. Feng, H. Wu, and M. Chen, "Analogy circuit synthesis and dynamics confirmation of a bipolar pulse current-forced 2D Wilson neuron model," *Eur. Phys. J. Special Topics*, vol. 230, nos. 7–8, pp. 1989–1997, Aug. 2021, doi: 10.1140/EPJS/S11734-021-00183-0.

[28] I. Apicella, S. Scarpetta, L. de Arcangelis, A. Sarracino, and A. de Candia, "Power spectrum and critical exponents in the 2D stochastic Wilson–Cowan model," *Sci. Rep.*, vol. 12, no. 1, p. 21870, Dec. 2022, doi: 10.1038/S41598-022-26392-8.

[29] Z. Ju, Y. Lin, B. Chen, H. Wu, M. Chen, and Q. Xu, "Electromagnetic radiation induced non-chaotic behaviors in a Wilson neuron model," *Chin. J. Phys.*, vol. 77, pp. 214–222, Jun. 2022, doi: 10.1016/J.CJPH.2022.03.012.

MOHAMMED ABDEL-HAFEZ (Senior Member, IEEE) received the B.Sc., M.Sc., and Ph.D. degrees in electrical and electronic engineering from Eastern Mediterranean University (EMU), Northern Cyprus, Turkey, in June 1992, August 1994, and November 1997, respectively. From 1992 to 1997, he was a Research Engineer with the Department of Electrical and Electronic Engineering, EMU. In 1995, he was an Instructor with the Department of Electrical Engineering, Al-Quds University. From 1997 to 1999, he was a Senior Manager with Palestine Telecommunication Company. In August 1999, he joined the Centre for Wireless Communications, University of Oulu, Oulu, Finland, as a Senior Research Scientist and the Project Manager. He is an Associate Professor of electrical and communication engineering with United Arab Emirates University, United Arab Emirates. He is also a Frequent Visiting Scientist with the Centre for Wireless Communications, University of Oulu. He has published more than 90 scientific publications. His research interests include modeling, design, and performance analysis of wireless communication systems; signal processing and system modeling; radio access; cooperative and relay networks; NOMA system; RF and microwave technologies; cognitive radio networks; and UWB communication.

FAWWAZ HAZZAZI (Member, IEEE) was born in Al-Kharj, Riyadh, Saudi Arabia. He received the B.S. degree in electrical engineering from Prince Sattam Bin Abdulaziz University-affiliated College of Engineering, Al-Kharj, the M.S. degree in electrical and computer engineering from the University of Maine, Orono, USA, and the Ph.D. degree in electrical engineering from Louisiana State University, in Baton Rouge, LA, USA. He has both industry and academic experience. His current research focuses on the characterization and fabrication of nanomaterials for the production of nanoscale electronic applications and electronic sensors of the next generation.

LEWIS NKENYEREYE received the Ph.D. degree in information security from Pukyong National University, Busan, South Korea. He was a Research Fellow with the Creative Human Resource Development Program for IT Convergence, Pusan National University. He was a Visiting Scholar with Thompson Rivers University, Kamloops, BC, Canada, and Georgia Southern University, Statesboro, GA, USA. He is currently an Assistant Professor of computer and information security with the Department of Computer and Information Security, College of Electronics and Information Engineering, Sejong University, Seoul, South Korea. His research spans across the wide range of security and privacy related techniques, with a particular interest in the Internet of Things (specifically the Internet of Vehicles). He is also involved in privacy-preserving techniques projects for blockchain-based applications and interoperability challenges in the IoT and M2M standards (with a special focus on one M2M). He has served as a member for several technical program committees in various conferences and journals.

IBRAHIM MAHARIQ (Member, IEEE) received the degree from the Department of Electrical and Computer Engineering, Palestine Polytechnic University, in 2003, the M.Sc. degree in electrical machines and the first Ph.D. degree in computational electromagnetics from Middle East Technical University, Ankara, Turkey, in 2009 and 2014, respectively, and the second Ph.D. degree in electrical engineering from TOBB Economic and Technology University, in 2017. In 2018, he was promoted to an Associate Professor, and currently with the Department of Electrical and Computer Engineering, Gulf University for Science and Technology (GUST). He has authored over 120 research articles. He is serving as the Chair for GUST Engineering and Applied Innovation Research Centre (GEAR), fostering innovation and research at the university.

MUHAMMAD AKMAL CHAUDHARY (Senior Member, IEEE) received the master's and Ph.D. degrees in electrical and electronic engineering from Cardiff University, Cardiff, U.K., in 2007 and 2011, respectively, and the M.B.A. degree in leadership and corporate governance from Edinburgh Business School, Heriot-Watt University, Edinburgh, U.K., in 2022. Before joining Ajman University, United Arab Emirates, in 2012, he held a postdoctoral research position with the Centre for High-Frequency Engineering, Cardiff University. He is currently an Associate Professor of electrical engineering with Ajman University. His research interests include nonlinear device characterization, spectrum-efficient power amplifiers, nonlinear measurement techniques, and microwave electronics, which have resulted in over 100 academic articles. He is a Chartered Engineer of the Engineering Council, U.K.; and a fellow of the Higher Education Academy, U.K.

MAHER ASSAAD received the master's degree in electrical engineering/microelectronics IC design from the University of Montreal, Montreal, Canada, in 2002, and the Ph.D. degree in electrical engineering/microelectronics IC design from the University of Glasgow, Glasgow, U.K., in 2009. He was a Senior Lecturer of electrical engineering with the University Technology of PETRONAS, Malaysia; and an Associate Professor of electronic and communication engineering with the American University of Ras Al Khaimah, United Arab Emirates. He is currently a Professor of electrical and computer engineering with Ajman University, United Arab Emirates. His research interests include the design of circuits/integrated circuits for various type of sensors and wireline and optical communication systems.